SYNTHESIS, CHARACTERIZATION, DFT, MOLECULAR DOCKING, AND IN VITRO SCREENING OF METAL CHELATES INCORPORATING SCHIFF BASE

Khansaa Shakir AL-Nama[*], Israa Adnan Saeed, Amera Faris Mohammed

University of Mosul, College of Science, Department of Chemistry, Nineveh-Iraq

ABSTRACT. The new complexes were formed by reacting Mn(II), Co(II), Ni(II), and Cu(II) with unsymmetrical Schiff base ligands, HL^1 and HL^2 , in a [1M:1L] molar ratio. Complexes were synthesized with high yields. Metal chelate structures were identified through FT-IR, elemental analyses, magnetic moment, and molar conductivity measurements. According to FT-IR findings, the Schiff base ligand HL^1 acts as tridentate by binding with metal ions, confirming tetrahedral geometry. While the ligand HL^2 is tetradentate, magnetic moment research indicated an octahedral structure. Theoretical calculations were performed using DFT. The synthesized complexes were tested for antibacterial activity against two types of Gram-positive bacteria: *S. aureus* and Gram-negative *K. pneumoniae*. Further molecular docking analysis revealed information about the ligand's binding energy and interaction with the protein receptor (ID:3BFV) of the bacteria.

KEY WORDS: Unsymmetrical Schiff base, Antibacterial activity, Molecular docking, DFT

INTRODUCTION

The compound with (R-CH=N-) (azomethine group) refers to the Schiff bases, discovered by Schiff in 1864 [1]. This type of compound is typically produced through a condensation reaction between a primary amine and an active carbonyl compound [2]. The interaction between an enzyme and the carbonyl or amino group of the primary reaction materials has identified Schiff bases as significant intermediates in enzymatic reactions [3]. Schiff base ligands, containing oxygen and nitrogen donors, are commonly used in coordination chemistry. These ligands can act as NO bidentate, NO2 tridentate, and N2O2 tetradentate donor agents [4, 5]. Unsynchronized polydentate Schiff bases are structured supramolecular metal complexes facilitated by metal ions. They have binding site cavities for various cations, anions, and organic molecules. Some of these complexes include N- and O-donor atoms, acting as effective stereospecific catalysts for oxidation, reduction, hydrolysis, bioactivity, and other transformations [6-9]. They are valuable models for researching metal-ligand interactions in metalloproteins and metalloenzymes [10]. Certain forms of these complexes exhibit interesting physical, chemical, and potentially beneficial chemotherapeutic properties [11]. The objective of this study is to synthesize unsymmetrical Schiff bases that contain (N) and (O) donor atoms and subsequently to prepare their transition metal complexes with Mn(II), Co(II), Ni(II), and Cu(II). The binding affinity of ligands to *Staphylococcus* CapA, a tyrosine kinase, was predicted using molecular docking (PDBID: 3BFV). It is a membrane protein structure. It was previously believed that bacteria were bereft of tyrosine-phosphorylating enzymes. In contrast to their eukaryotic counterparts, numerous varieties of tyrosine kinases have been recently identified in bacteria. They are involved in a variety of physiological processes. It is still unclear what their precise functions are due to the sluggish progress in their structural characterization. It has been defined as a co-polymerase that is capable of producing and exporting extracellular polysaccharides. Bacterial tyrosine kinases are potential therapeutic targets due to the critical role that this type of compound plays in the virulence of

————————

*Corresponding authors. E-mail: khnsaash.al-nama@uomosul.edu.iq

pathogenic bacteria [12]. The analysis of interactions between the protein and substrate was used to calculate binding energies. The ligands' prospective physiological effects and their potential utility for a variety of medical applications in the future are suggested by the promising results.

EXPERIMENTAL

Materials

Chemicals were purchased from Sigma-Aldrich and Fluka and used without further purification. Mn(II) chloride, Co(II) chloride, Ni(II) chloride, and Cu(II) chloride, glacial acetic, acenaphthoquinone, benzil, 2-aminophenol, and 2-aminobenzophenone, as well as organic solvents such as ethanol, dimethylformamide (DMF), and dimethyl sulfoxide (DMSO), were spectroscopically grade obtained from BDH Chemicals.

HL1 and HL2 Schiff base ligands preparation

Step 1. Synthesis of 2-((2-hydroxyphenyl) imino) acenaphthylen-1(2H)-one (A1)
           Synthesis of 2-((2-hydroxy phenyl) imino)-1,2-diphenylethan-1-one (A2)

A mixture of acenaphthoquinone (0.91 g, 5 mmol) and/or benzil (1.05 g, 5 mmol) and (0.54 g, 5 mmol) of 2-aminophenol in (20 mL) of absolute ethanol with the addition of a few drops of glacial acetic acid was refluxed with stirring for 4 h [13]. The content was concentrated to half of the volume and allowed to cool. The product separated on evaporation of the solvent was filtered, washed with alcohol, and then finely recrystallized from ethanol to give the target compound (A1).

Compound (A1). Green solid, m.p.: 210-215 °C; yield: 81%; C.H.N. cal. (found) C%; 79.1 (78.33), H%; 4.02 (4.55), N%; 5.11 (5.51). FT-IR (cm^{-1}): 3353 (OH, stretch), 1725 (C=O, stretch), 1619 (C=N, stretch).

Compound (A2). Pale yellow solid, m.p. 250-252 °C; yield: 77%; C.H.N. cal. (found) C%; 79.7 (78.00), H%; 4.98 (4.15), N%; 4.65 (4.00). FT-IR (cm^{-1}): 3385 (OH, stretch), 1715 (C=O, stretch), 1626 (C=N, stretch). The pathway of the compounds (A1, 2) is shown in Scheme 1.

Step 2. Synthesis of Schiff base ligands

2-((2-Hydroxyphenyl)imino)acenaphthylen-1(2H)-ylidene) amino) phenyl) (phenyl) methanone (HL1). 2-((2-hydroxyphenyl)imino)-1,2-diphenylethylidene)amino)phenyl)(phenyl)methanone (HL^2). A mixture of (A1) (0.54 g, 2 mmol) and/or (A2) (0.6 g, 2 mmol) in (20 mL) of absolute ethanol was refluxed and stirred with (0.39 g, 2 mmol) of 2-aminobenzophenone for 6 h. The product separated on evaporation of the solvent was filtered, washed with alcohol, and then finely recrystallized from ethanol to give the target compounds. The pathway is shown in Scheme 1.

HL1. ^{1}H NMR (400 MHz, DMSO-d$_6$) δ: 9.87 (s, 1H, OH phenolic), 8.49 (dd, J = 7.4, 1.1 Hz, 1H, Ar-H), 8.05 (dd, J = 7.4, 1.1 Hz, 1H, Ar-H), 7.98 (dd, J = 8.4, 1.1 Hz, 1H, Ar-H), 7.89 – 7.83 (m, 2H, Ar-H), 7.76 – 7.67 (m, 3H, Ar-H), 7.65 (dd, J = 8.3, 1.2 Hz, 1H, Ar-H), 7.60 – 7.53 (m, 1H, Ar-H), 7.46 – 7.36 (m, 2H, Ar-H), 7.28 – 7.21 (m, 1H, Ar-H), 7.07 (dd, J = 7.8, 1.5 Hz, 1H, Ar-H). FT-IR (cm^{-1}): 3421 (OH, stretch), 1716 (C=O, stretch), 1645, 1600 (C=N, stretch).

HL2. ^{1}H NMR (400 MHz, DMSO-d6) δ 9.96 (s, 1H, OH phenolic), 8.62 (dd, J = 7.6, 1.9 Hz, 2H, Ar-H), 8.48 – 8.37 (m, 1H, Ar-H), 8.31 – 8.20 (m, 2H, Ar-H), 7.86 (dd, J = 7.8, 1.5 Hz, 2H, Ar-H), 7.76 – 7.62 (m, 4H, Ar-H), 7.56 – 7.40 (m, 3H, Ar-H), 7.17 (dd, J = 7.1, 1.5 Hz, 2H,

Ar-H), 7.03 (dd, J = 7.9, 1.7 Hz, 1H, Ar-H). FT-IR (cm^{-1}): 3379 (OH, stretch), 1720 (C=O, stretch), 1691, 1601 (C=N, stretch).

Metal chelates preparation

The Schiff base ligand HL^1 (0.45 g, 1 mmol) and/or ligand HL^2 (0.48 g, 1 mmol) were dissolved in ethanol. The following ethanolic metal salt solutions were added to the ligand solution at the molar ratio (1L:1M): 0.394 g Mn(II), 0.2379 g Co(II), 0.2377 g Ni(II), and 0.1704 g Cu(II). The mixture was refluxed and stirred for 4 h at 75 °C. The product was filtered and washed with a solution of water-EtOH (1:2) and petroleum ether. The synthesized compounds were dried in desiccators with anhydrous CaCl₂ in a vacuum desiccator and subsequently purified through recrystallization with methanol [7, 9], Scheme 1.
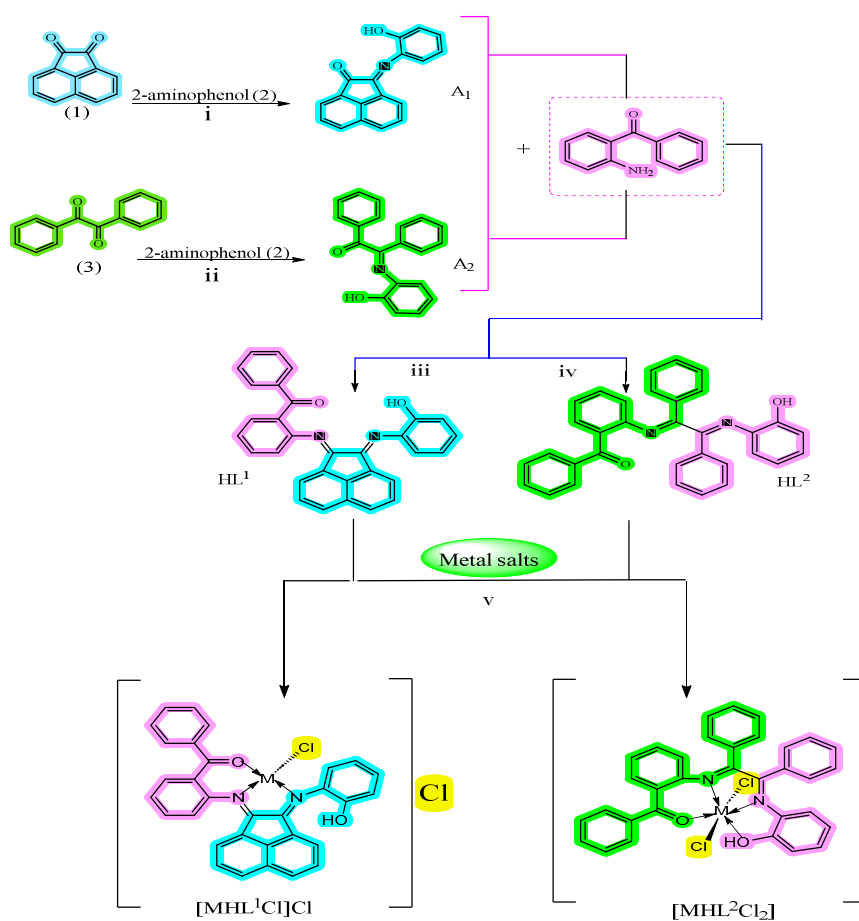
M= Mn(II), Co(II), Ni(II) and Cu(II)

Scheme 1. Preparation of the ligands (HL^1, HL^2) and their metal complexes.

Reagents and conditions: (i) abs. EtOH, Gla.CH$_3$CO$_2$H, reflux for 4 h, (ii) abs. EtOH, Gla.CH$_3$CO2H, reflux for 4 h, (iii) abs. EtOH, reflux for 6 h, (iv) abs. EtOH, reflux for 6 h, (v) abs. EtOH reflux for 4 h.

Instrumentation

The study employed a variety of physical and spectral methodologies to characterize all compounds. The IR- spectroscopy was conducted using the FT-IR spectrometer from Bruker and the JASCO canvas FT-IR 4200 (with KBr disk) in wavenumber (400–4000 cm^{-1}). ^{1}H NMR spectra were determined on Bruker Bio Spin GmbH (400 MHz); tetramethyl silane was used as an internal reference, and chemical shifts are quoted in δ (ppm). The samples' conductivity was measured using a HANNA EC214 conductivity meter. The Euro EA Elemental Analysis Euro 3000 (Italy) was used to record the elemental analysis (C.H.N.). The atomic absorption spectrophotometer model Sense AAGCB scientific apparatus (3000 System) was employed to conduct the metal center analyses. To determine the (m.p.), an electrothermal melting point (9100) was used. Measurements of magnetic susceptibility were carried out by Sherwood (MKI), by Shimadzu 1800 spectroscopy, and the electronic spectra were recorded in DMF (UV-Vis) spectrophotometer type UV analytikjephotometer.

Antibacterial activity

HL^1 and HL^2 and their complexes were tested for antibacterial activity using the agar diffusion method. Nutrient agar on Petri dishes was used to culture *S. aureus* and *K. pneumonia*. Test solutions were prepared by dissolving 10.0 mg of each sample in 1.0 mL of DMSO. Filter paper discs soaked in the solution were used, and after 24 hours at 37 °C, inhibition zone diameters were measured [12].

Molecular docking study

PDB (ID 3BFV) was used to obtain the three-dimensional protein structure (bacterial enzyme in membrane protein CapA1, tyrosine kinase PDB format). The aforementioned platform performed Vina's docking [14]. The x, y, and z values (as required to specify the position of the docking grid) were entered into the workflow as 116739, 11.4154, and 25.2909, respectively. The protein and ligands were prepared using AutoDock Tools (ADT) 1.5.6. Following the removal of the native ligands and crystallographic water molecules from the PDB structures, the polar hydrogens were subsequently added before the docking process. ChemAxon Marvin Sketch 5.3.735 produced the ligands' conformations and structures, which were saved in the mol2 format. The Avogadro v1.2.0 software was applied to optimize and minimize the energy of ligand structures. DS (Discovery Studio Visualizer, v4.0.100.13345) was utilized for the analysis of protein-ligand interactions and the graphical display of the computed findings [15, 16].

DFT modeling study

At times, the lack of a crystal structure necessitated computer investigations to gain a better understanding of the molecular structures of the ligand and its complexes. The GW9 Gaussian 16 program was utilized to conduct geometric optimizations. The singlet ground state molecular geometries in the gas phase were extensively optimized at the B3LYP theoretical level for the complexes. Figure 4 utilized LANL2DZ to represent Mn(II), Co(II), Ni(II), and Cu(II) atoms, while the ligand atoms were modeled with the 6-311 (d,p) basis set. During the study, it was discovered that the compounds had ideal geometries, and their molecular edge orbitals, including the LUMO and HOMO, were determined. The HOMO and LUMO energies, shown in Figures 7 and 8, were used to compute the values of chemical hardness (η), softness (σ), electronegativity (χ), energy gap (ΔE), nucleophilicity (η), maximum electronic charge (ΔNmax), and electrophilicity index (ω) [17-19]. Table 4 presents the results of the computation.

RESULTS AND DISCUSSION

Structure configuration of the ligands

The prepared ligands were characterized using elemental analysis, FT-IR, and ^{1}H-NMR spectra. In the FT-IR spectra for HL[1] and HL[2], bands at 1716 and 1720 and at 3379 and 3421 cm^{-1} were observed, referring to ν(C=O) and ν(OH) frequencies, respectively. On the other hand, the -NH$_2$ group disappeared from the starting materials, and new bands related to the imine -C=N group emerged at ν(C=N) for the imine groups at 1600, 1645 cm^{-1} and at 1602, 1691 cm^{-1}, respectively [19-24]. The ^{1}H-NMR spectrum in DMSO-d6 showed signals for the -OH group at δ 9.87 and 9.96 ppm and for the aromatic protons (-C=CH-) group at δ 8.62-7.03 ppm [20-22]. The integration in the spectrum of ^{1}H-NMR for the HL[1] ligand refers to 2H protons in the phenyl group and 3H protons in the acenaphthoquinone group. The integration in the spectrum of ^{1}H-NMR for the HL[2] ligand indicates that 6H protons are symmetrical in the three phenyl groups.

Table 1. Physical properties, conductivity, and analysis information of the synthesized compounds.

No.	Compound	Colour	m.p. °C	C.H.N. cal. (found)			M% cal. (found)	Conductivity ohm^{-1}.cm^{-1}.mol^{-1}
				C%	H%	N%		
HL[1]	$C_{31}H_{20}O_2N_2$	Dark green	240	82.30 (81.11)	4.42 (4.91)	6.91 (6.91)	-----	-----
1	[MnHL[1]Cl]Cl	Yellow	182	64.37 (69.00)	3.46 (3.00)	4.84 (3.91)	9.49 (9.00)	34.2
2	[CoHL[1]Cl]Cl	Blue	179	63.92 (61.29)	3.43 (2.98)	4.81 (4.00)	10.12 (9.24)	44.1
3	[NiHL[1]Cl]Cl	Brown	128	63.9 (61.99)	3.43 (2.80)	4.81 (3.81)	10.08 (9.11)	34.9
4	[CuHL[1]Cl]Cl	Dark brown	195	63.42 (62.00)	3.41 (2.70)	4.77 (3.9)	10.81 (9.41)	30.6
HL[2]	$C_{33}H_{24}N_2O_2$	Greenish brown	145	82.50 (80.91)	5.00 (4.69)	5.83 (6.81)	-----	-----
5	[MnHL[2]Cl$_2$]	Yellowish white	111	64.24 (62.00)	3.89 (2.91)	4.54 (5.00)	10.60 (10.99)	20
6	[CoHL[2]Cl$_2$]	Yellowish green	132	64.92 (62.91)	3.93 (3.01)	4.59 (4.01)	9.66 (7.90)	15
7	[NiHL[2]Cl$_2$]	Brown	170	64.95 (63.10)	3.93 (3.11)	4.59 (4.00)	9.62 (8.26)	17.8
8	[CuHL[2]Cl$_2$]	Light brown	185	64.44 (63.20)	3.90 (3.00)	4.55 (3.79)	10.33 (11.51)	21.7

Structure configuration of the complexes

The synthesized complexes were soluble in common organic solvents such as acetone, DMF, and DMSO, but they were insoluble in water. The findings of the microanalysis for the metal complexes (CHN) showed good agreement between the calculated and observed values, confirming the proposed formula in Table 1. The conductivity measurements were carried out using DMSO as a solvent for a 10^{-3} M concentration at 25°C. These results indicate that complexes no. (2-4), which were prepared from HL[1], appeared to be 1:1 electrolytes, while complexes no. (5-8), which were prepared from HL[2], appeared to be nonconductive, as shown in Table 1. On the other hand, the geometrical shape of complexes no. (1-4) is tetrahedral, while for complexes no. (5-8), they are octahedral, which is suggested based on the magnetic properties and the spectral data, in good agreement with what has been mentioned in the literature [18-21]. Table 2 includes the magnetic results as well as spectral band values and their transition bands.

Table 2. Magnetic moments and electronic spectra data of synthetic complexes.

No.	μ_{eff} (B.M)	Bands cm^{-1}	Suggested transition	Geometry
HL^1	-----	45789, 41002	$\pi \rightarrow \pi^*$, $n \rightarrow \pi^*$	
1	5.60	47870, 41800, 32791	$\pi \rightarrow \pi^*$, $n \rightarrow \pi^*$, C.T	T.d
2	3.46	46442, 32011, 30916, 16107, 12443	$\pi \rightarrow \pi^*$, $n \rightarrow \pi^*$, C.T $^4A_2(F) \rightarrow {}^4T_1 (P)$, $^4A_2(F) \rightarrow {}^4T_2(F)$	T.d
3	3.01	44671, 39611, 29115, 16278, 13007	$\pi \rightarrow \pi^*$, $n \rightarrow \pi^*$, C.T $^3T_1(F) \rightarrow {}^3T_2(F)$; $^3T_1(F) \rightarrow {}^2A_2(F)$ C.T	T.d
4	2.00	46741, 43219, 29917, 12009	$\pi \rightarrow \pi^*$, $n \rightarrow \pi^*$, C.T $^2Eg \rightarrow {}^2T_2g$	T.d
HL^2	-----	47161, 41850, 32901	$\pi \rightarrow \pi^*$, $n \rightarrow \pi^*$, C.T	
5	5.25	46171, 45590, 31957	$\pi \rightarrow \pi^*$, $n \rightarrow \pi^*$, C.T	O.h
6	4.05	46827, 36140, 31582, 20091, 15971, 13260	$\pi \rightarrow \pi^*$, $n \rightarrow \pi^*$, C.T $^4Tig(F) \rightarrow {}^4Tig(F)$, $^4Tig(F) \rightarrow {}^4A_2g(F)$, $^4T_1g(P)$	O.h
7	2.79	46012, 39487, 31002, 21309, 154611, 12099	$\pi \rightarrow \pi^*$, $n \rightarrow \pi^*$, C.T $^3A_2(g)(F) \rightarrow {}^3T_2g(F)$, $^3A_2g(F) \rightarrow {}^3T_1g(F)$, $^3A_2g(F) \rightarrow {}^3T_1g(P)$	O.h
8	1.91	41532, 38610, 29332, 12793	$\pi \rightarrow \pi^*$, $n \rightarrow \pi^*$, C.T $Eg \rightarrow {}^2T_2g$	O.h
		* CT = Charge transition, T.d = Tetrahedral, O.h = Octahedral		

Table 3. Personalized FT-IR bands of ligands and their complexes.

No.	Compound	ν (C=N) cm^{-1}	ν (C=O) cm^{-1}	ν (OH) cm^{-1}	ν (M-O) cm^{-1}	ν (M-N) cm^{-1}
HL^1	$C_{31}H_{20}O_2N_2$	(1645, 1600)	1716	3421	---	---
1	[MnHL^{1}Cl]Cl	(1620, 1580)	1715	3420	612	493
2	[CoHL^{1}Cl]Cl	(1602, 1587)	1720	3421	507	432
3	[NiHL^{1}Cl]Cl	(1630, 1580)	1723	3420	598	501
4	[CuHL^{1}Cl]Cl	(1610, 1582)	1725	3491	600	445
HL^2	$C_{33}H_{24}N_2O_2$	(1691, 1602)	1720	3379	----	----
5	[MnHL^{2}Cl$_2$]	(1633, 1590)	1710	3360	501	442
6	[CoHL^2 Cl$_2$]	(1645, 1589)	1711	3321	543	491
7	[NiHL^2 Cl$_2$]	(1654, 1590)	1708	3310	520	456
8	[CuHL^2 Cl$_2$]	(1660, 1587)	1708	3396	504	444

IR spectra results are one of the most important measurements to identify the effective groups in the ligand and thus identify the method of coordination between the ligand and central atom. Due to the asymmetric electronic nature of ligands, two bands were observed for ν(C=N) imine groups at (1645, 1600) cm^{-1} and (1691, 1602) cm^{-1} for HL^1 and HL^2, respectively [22-25]. Other bands at (1716, 1720) cm^{-1} and (3421, 3379) cm^{-1} refer to ν(C=O) and ν(OH) frequency, respectively [19, 24]. In the spectrum of complexes (1-4) prepared from HL^1, ν(C=N) stretching frequency shifted to a lower frequency. This shift in this group band indicates a coordination site from the (nitrogen atoms) of imine groups in the ligands [22, 23]. On the other hand, ν(C=O) stretching frequency shifted to higher or lower frequency refers to coordination from the (oxygen atom) of carbonyl group [25]. Band ν(OH) appeared in almost the same location and sharp, which indicates that HL^1 may coordinate as a tridentate ligand through the N atoms of imine groups and (oxygen atom) of ketone carbonyl group, while the oxygen atom of the hydroxide group did not

share inconsistency. This is likely that these complexes have a structural formula [MHL^{1}Cl] Cl, while the spectra of complexes (5-8) prepared from HL^2 the position of ν(OH) band was changed compared with the spectrum of the ligand indicating that HL^2 may coordinate as a tetradentate ligand through the (nitrogen atoms) of imine groups and (oxygen atoms) of ketone carbonyl group as well as hydroxide group, this may indicate that these complexes have a structural formula [MHL^{2}Cl$_2$].

The results of antibacterial activity

Except for HL^1 and HL^2, which showed good activity toward *S. aureus* bacteria, all other compounds prepared in this work showed activity toward both types of bacteria that can be described as medium to weak compared with the standard sample ciprofloxacin, as shown in Figure 1.
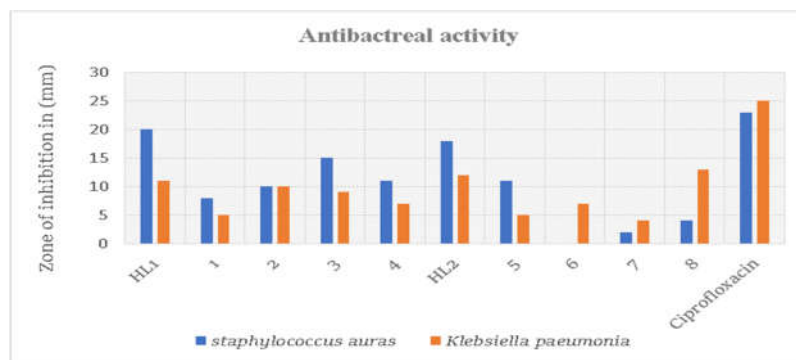
Figure 1. Antibacterial activity of ligands and their complexes.

Molecular docking

Molecular docking, an essential technique in the structural design process, can facilitate and accelerate drug discovery. The current study investigated the interactions of several inhibitors with the Staphylococcus receptor utilizing molecular docking. In this study, we performed molecular docking screening of synthesized ligands HL^1 and HL^2. After obtained the coordinate crystal of the tyrosine kinase protein (PDB ID: 3BFV) and measured the binding affinities of the synthesized compounds toward tyrosine kinase. Hydrophobic interactions occurred with amino acid residues ARG:238, ILE: 114, PHE:25, and SER:82 through carbon-hydrogen bonds. The protein is stabilized by two conventional hydrogen bond interactions, THR:83 and THR:110. Meanwhile, HL^2 shows hydrophobic interactions with amino acid residues such as ILE:114, ARG:238, and PHE:25 through the carbon-hydrogen bond SER:32. The protein is stabilized by two conventional hydrogen bond interactions, ASN:237 and THR:83. Additional data reveal 2D interactions between ligand and amino acids in the enzyme pocket. The enzyme's aromatic amino acids surrounding ligand, solvent accessibility (SAS), aromatic amino acids around ligand in the enzyme pocket, ionizability, hydrophobicity, H-bonds, and interpolated charge are depicted in Figures 2 and 3. According to the molecular docking investigation, HL^2 has improved docking scores compared to HL^1 (-7.0 and -7.4 kcal/mol, respectively). This finding confirms the hypothesis that docking studies may further our understanding of how molecules attach to enzymes [25].
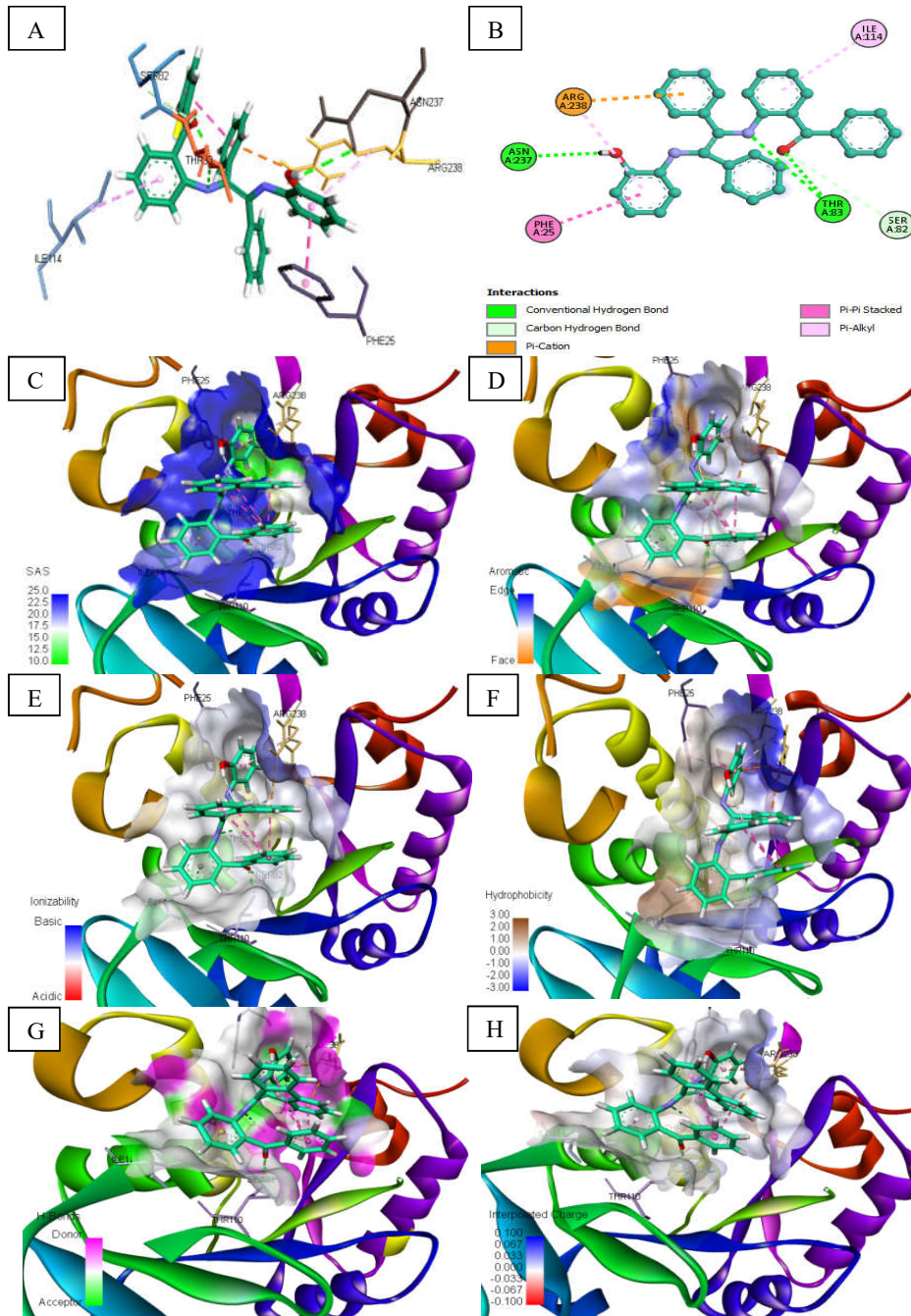
Figure 2. (A) 3D interaction between compound HL[1] and amino acid in the pocket of (ID: 3BFV) enzyme. (B) 2D interaction between HL[1] and (ID: 3BFV) enzyme. (C) Solvent accessibility (SAS). (D) Aromatic amino acid around the HL[1] in the pocket of (ID: 3BFV). (E) Ionizability amino acid around the HL[1] in the pocket of (ID: 3BFV). (F) Hydrophobicity. (G) H-bonds between the amino acid and HL[1] in the pocket of (ID: 3BFV) (H) Interpolated charge around the HL[1] in the pocket of (ID: 3BFV).
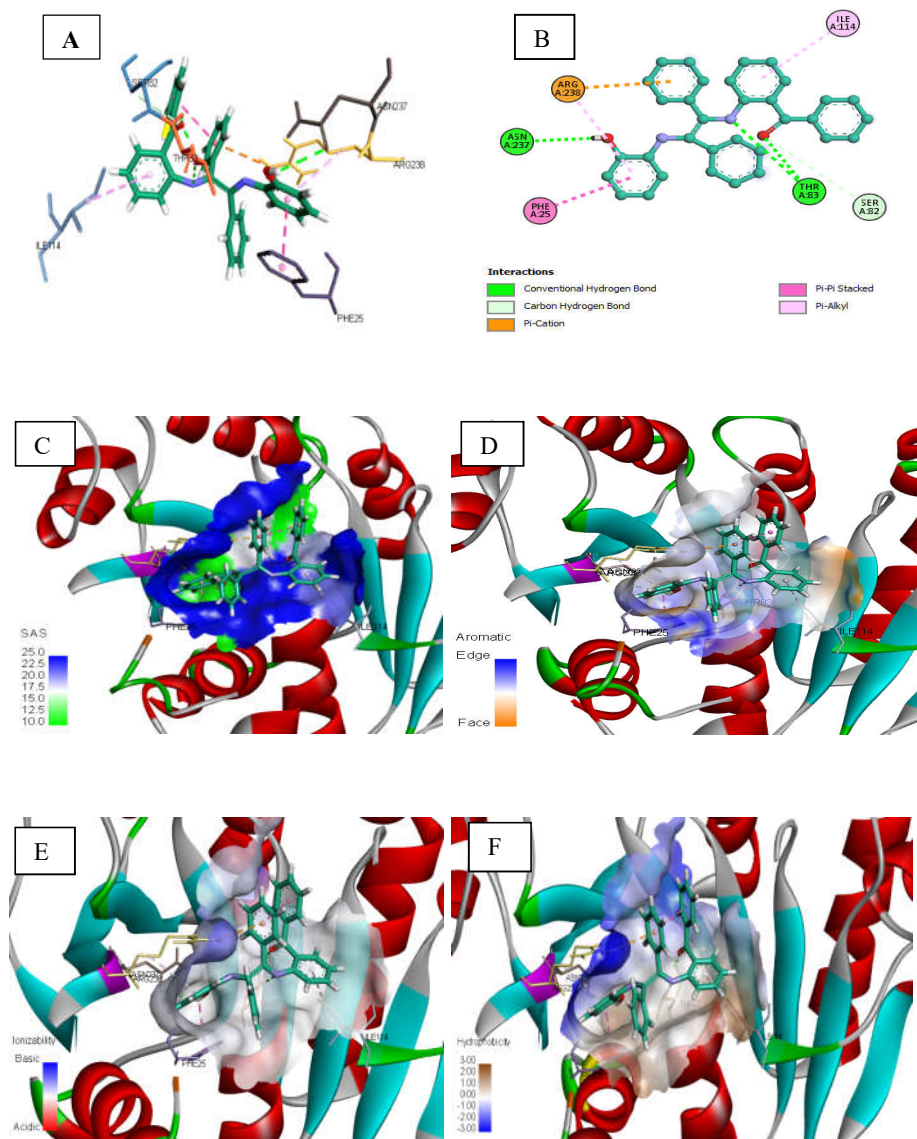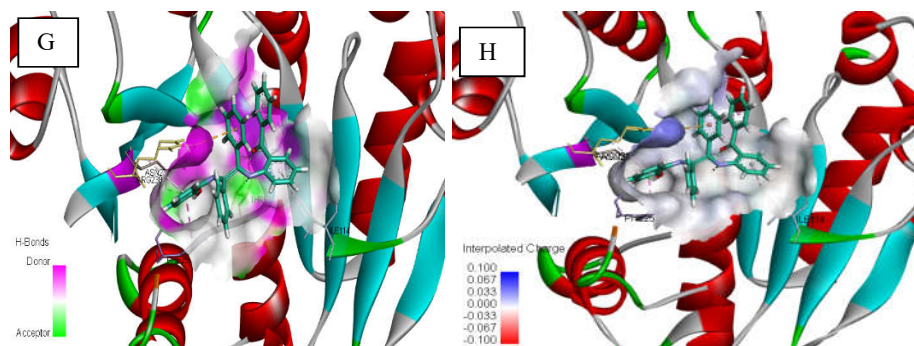
Figure 3. (A) 3D interaction between compound HL^2 and amino acid in the pocket of (ID: 3BFV) enzyme. (B) 2D interaction between HL^2 and (ID:3BFV) enzyme. (C) Solvent accessibility (SAS). (D) Aromatic amino acid around the HL^2 in the pocket of (ID: 3BFV). (E) Ionizability amino acid around the HL^2 in the pocket of (ID:3BFV). (F) hydrophobicity. (G) H-bonds between the amino acid and HL^2 in the pocket of (ID: 3BFV) (H) Interpolated charge around the HL^2 in the pocket of (ID: 3BFV).

Calculation of density functional theory (DFT)

The calculation was carried out using the Gaussian (G16) program, which is successful for organic and coordination compounds, while GaussView 4.1 is used to draw the structures [19]. The basis set atoms and 6-311G-(D, P) for each atom, C, N, O, and H, are used to optimize the free ligands and their complexes at the B3LYP level. It is suggested that the size of the gap itself may be a valuable indicator of hardness, given the recognition that hard acids and bases have a large HOMO-LUMO gap. Consideration of Pearson's definition of η by the subsequent equation may serve as the foundation for this concept:

$$n = \frac{1}{2}\left(\frac{\partial \mu}{\partial N}\right)\vartheta(r) \qquad (1)$$

(μ) is defined by DFT as the following equation:

$$\mu = \left(\frac{\partial E}{\partial N}\right)\vartheta(r) \qquad (2)$$

where e = energy and N = number of electrons of the system under external pressure $\vartheta(r)$. Both (μ and η) can be calculated based on the term of ionization potential (I.P.) and electron affinity (E A) as shown in these equations:

$$\mu = -\left(\frac{IP+EA}{2}\right) \text{ and } n = \left(\frac{IP-EA}{2}\right) \qquad (3)$$

The connection between Pearson's absolute hardness/softness and the HOMO - LUMO gap then follows from Koopmans theorem, in which the (IP) is just the opposite of HOMO energy, similarly, (EA), defined as the opposite of LUMO energy.

$$\mu = \left(\frac{E_{LUMO}-E_{HOMO}}{2}\right) \text{ and } n = \left(\frac{E_{LUMO}+E_{HOMO}}{2}\right) \qquad (4)$$

HL^1

HL^2

CoHL^1

NiHL^1

MnHL^2

CuHL^2
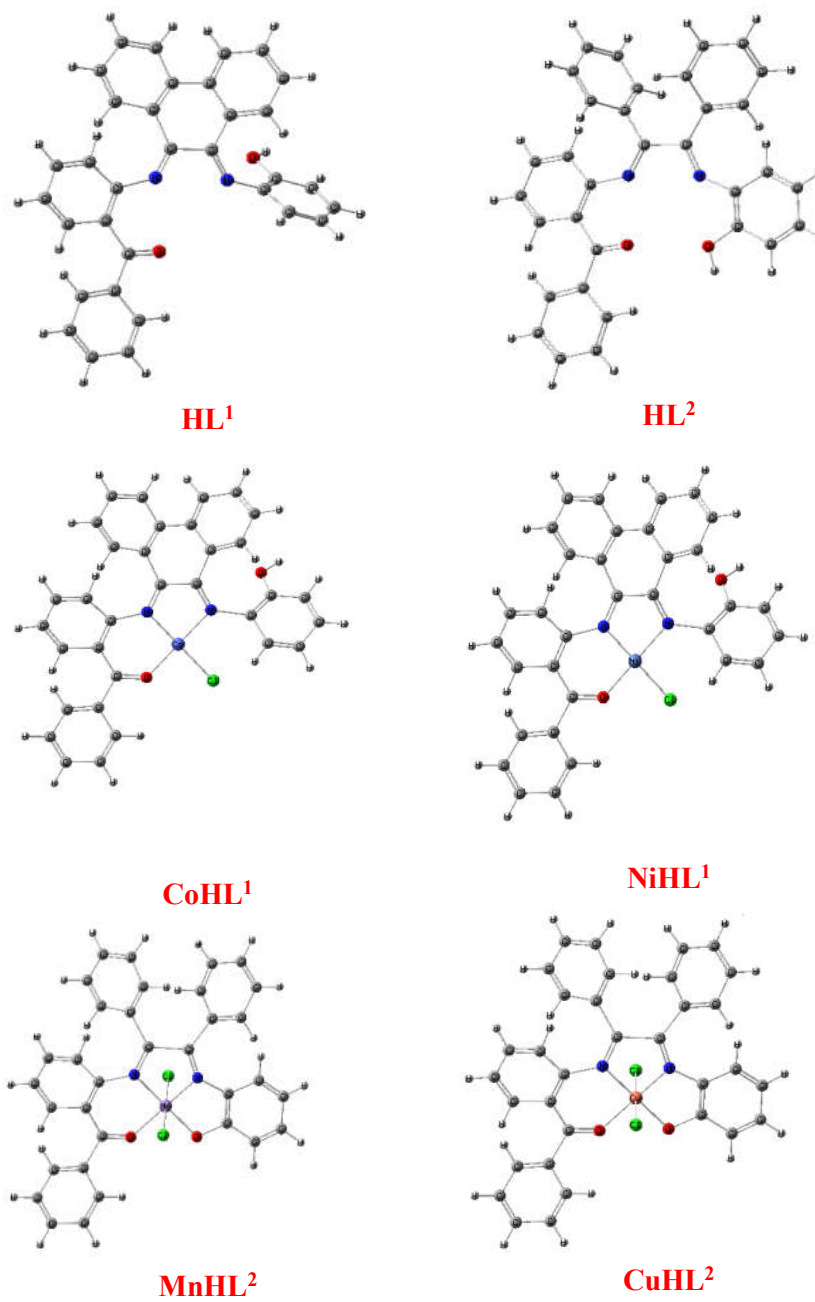
Figure 4. Optimized structures of ligands HL^1, HL^2, and some of their complexes.
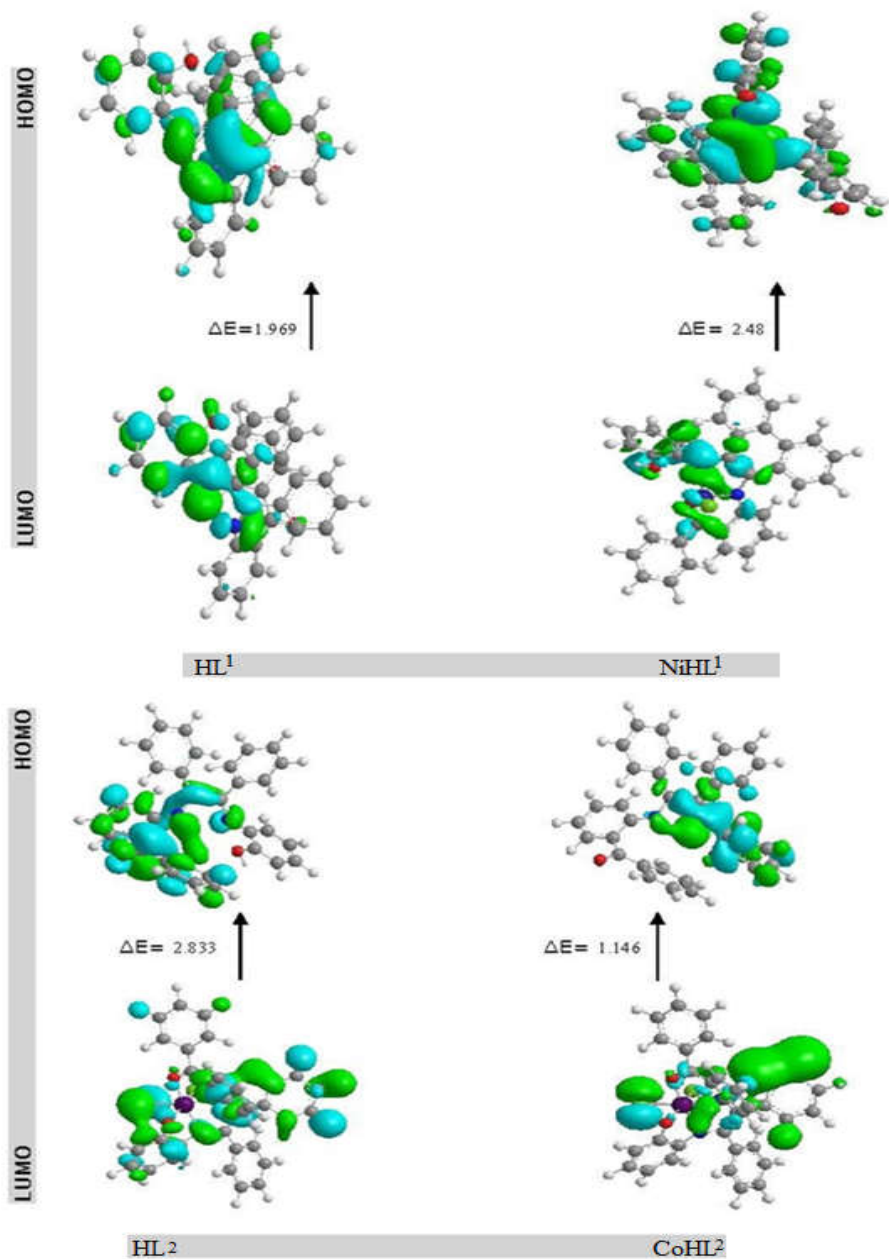
Figure 5. The HOMO-LUMO energy diagram of ligands HL^1, HL^2 and one of their synthesized complexes calculated at DFT/B3LYP/6-311G+(d,p) in the gaseous phase.

(ω) is defined by Parr and his team as a measure of electrophilicity power:

$$\omega = \frac{\mu^2}{2n} \tag{5}$$

The energy gap (ΔE) = [EHOMO – ELUMO].

$$\Delta N_{max} = -\ \mu/\eta\ [26\text{-}30] \tag{6}$$

All these parameters have been calculated for HL^1 and HL^2 and their complexes, recorded in Table 4. Analysing the boundary molecular orbital (HOMO) and (LUMO) is very necessary to know the properties and behaviour of the molecules such as the chemical hardness, softness, chemical reactivity, and kinetic stability [26, 27]. The stability of the compound has a minimum (ω) it has a maximum stability, so the stability order of the prepared compounds is as follows: $CoHL^1 >$ $MnHL^1 > NiHL^1 > HL^1 > CuHL^1$, $NiHL^1 > HL^2 > CuHL^2 > MnHL^2$. $CoHL^2$

The optimized structures and the HOMO and LUMO of HL^1, HL^2, $CoHL^2$, $NiHL^1$, $MnHL^2$ and $CuHL^2$ shown in Figures 4 and 5.

Table 4. Calculated the quantum chemical parameters of ligands and their complexes.

No.	E LUMO	E HOMO	$\triangle E$	X	H	Σ	Pí	Δ	Ω	$\triangle N_{max}$
HL^1	-6.216	-8.185	1.969	7.2005	0.9845	1.0157	-7.2005	0.507	26.3317	7.3138
$MnHL^1$	-5.155	-7.623	2.468	6.389	1.234	0.8103	-6.389	0.405	16.5394	5.1774
$CoHL^1$	-4.588	-6.913	2.325	5.7505	1.1625	0.8602	-5.7505	0.430	14.2229	4.9466
$NiHL^1$	-5.212	-7.692	2.48	6.452	1.24	0.8064	-6.452	0.403	16.7856	5.20321
$CuHL^1$	-8.45	-10.535	2.085	9.4925	1.0425	0.9592	-9.4925	0.479	43.2710	9.1055
HL^2	-4.929	-8.000	2.833	6.3455	1.4165	0.7059	-6.3455	0.352	14.2129	4.4797
$MnHL^2$	-5.561	-6.663	1.102	6.112	0.551	1.8148	-6.112	0.907	33.8766	11.0925
$CoHL^2$	-6.103	-7.249	1.146	6.676	0.573	1.7452	-6.676	0.872	38.8909	11.6509
$NiHL^2$	-6.128	-13.896	7.768	10.012	3.884	0.2574	-10.012	0.128	12.8909	2.5777
$CuHL^2$	-4.815	-5.728	0.913	5.2715	0.4565	2.1905	-5.2715	1.095	30.4367	11.5476

CONCLUSION

This work investigates the synthesis of unsymmetrical Schiff bases that act as tridentate ligand HL^1 complexes and tetradentate ligand HL^2 complexes in a molar ratio of 1:1 (M/L) for both types, with physicochemical and spectroscopic methods used to characterize their structures. According to the results, the HL^1 complexes exhibited tetrahedral geometry; the HL^2 complexes exhibited octahedral geometry. DFT with the B3LYP method was employed to predict the optimal geometries and frontier molecular orbitals of the complexes. In vitro screening was conducted to evaluate the antibacterial activity of the ligand and its complexes against pathogenic bacteria. The results of the antibacterial activity indicate that the free ligand exhibits greater antibacterial activity than the complexes. Furthermore, molecular docking was used to determine the bonding interactions between the ligand and the Staphylococcus aureus receptors (PDB ID: 3BFV). The active site was investigated using a molecular docking approach.

ACKNOWLEDGEMENTS

Disclosure statement

The authors declare that they have no competing interests.

REFERENCES

1. Qin, W.; Long, S.; Panunzio, M.; Biondi, S. Schiff bases: A short survey on an evergreen chemistry tool. *Mol*. **2013**, 18, 12264-12289.
2. Boulechfar, C.; Ferkous, H.; Delimi, A.; Djedouani, A.; Kahlouche, A.; Boublia, A.; Darwish, A.S.; Lemaoui, T.; Verma, R.; Benguerba, Y. Schiff bases and their metal complexes: A review on the history, synthesis, and applications. *Inorg. Chem. Commun*. **2023**, 150, p.110451.
3. Younus, H.A.; Saleem, F.; Hameed, A.; Al-Rashida, M.; Al-Qawasmeh, R.A.; El-Naggar, M.; Rana, S.; Saeed, M; Khan, K.M. Part-II: An update of Schiff bases synthesis and applications in medicinal chemistry-a patent review (2016-2023). *Expert Opin. Ther. Pat*. **2023**, 33, 841-864.
4. Nabhan, K.J.; Mahdi, A.S.; Al-Zaidi, B.H.; Ismail, A.H. Nasif, Z.N. New tetra-dentate Schiff base ligand N2O2 and its complexes with some of metal ions: Preparation, identification, and studying their enzymatic and biological activities. *Baghdad Sci. J.* **2022**, 19, 0155-0155.
5. Kargar, H.; Fallah-Mehrjardi, M.; Behjatmanesh-Ardakani, R.; Rudbari, H.A.; Ardakani, A.A.; Sedighi-Khavidak, S.; Munawar, K.S.; Ashfaq, M.; Tahir, M.N. Binuclear Zn(II) Schiff base complexes: Synthesis, spectral characterization, theoretical studies and antimicrobial investigations. *Inorg. Chim. Acta* **2022**, 530, 120677.
6. AL-nama, K.S.; AL Nidaa, E.M. Preparation and characterization of Co(II), Ni(II), Cu(II) and Zn(II) complexes with unsymmetrical tetradentate Schiff bases ligands. *J. Educ. Sci*. **2019**, 28, 2.
7. Nguyen, Q.T.; Pham Thi, P.N.; Nguyen, V.T. Synthesis, characterization, and in vitro cytotoxicity of unsymmetrical tetradentate Schiff base Cu(II) and Fe(III) complexes. *Bioinorg. Chem. Appl*. **2021**, 2021, p.6696344.
8. Hasan, H.A.; Mahdi, S.M.; Ali, H.A. Tetradentate azo Schiff base Ni(II), Pd(II) and Pt(II) complexes synthesis, spectral properties, antibacterial activity cytotoxicity and docking studies. *Bull. Chem. Soc. Ethiop*. **2024**, 38, 99-111.
9. Al-Jiboury, M.M.; Al-Nama, K.S. Preparation, characterization and biological activities of some unsymmetrical Schiff bases derived from m-phenyelenediamine and their metal complexes. *Rafidain J. Sci*. **2019**, 28, 23-36.
10. Ghasemi, L.; Behzad, M.; Khaleghian, A.; Abbasi, A.; Abedi, A. Synthesis and characterization of two new mixed-ligand Cu(II) complexes of a tridentate NN'O type Schiff base ligand and N-donor heterocyclic co-ligands: In vitro anticancer assay, DNA/human leukemia/COVID-19 molecular docking studies, and pharmacophore modeling. *Appl. Organomet. Chem*. **2022**, 36, e6639.
11. Gheibi, N.; Piri, H.; Hashemi, Z. Interaction of human serum albumin with methotrexate: Stability and structural analysis. *Int. J. Community Curr. Res.* **2017**, 43, 30-38.
12. Al burgus, A.F.; Ali, O.T.; Al-abbasy, O.Y. Design, synthesis and molecular docking of new spiro heterocyclic coumarin as antibacterial agents. *Rev. Roum. Chim*. **2024**, 69, 399-404.
13. Aljamali, N.; Hadi, M.; Mohamad, M.; Salih, L.; Aljamali, N. Review on imine derivatives and their applications. *Int. J. Pharmacogn. Phytochem. Res*. **2019**, 5, 20-32.
14. Sanner, M.F. Python: A programming language for software integration and development. *J. Mol. Graph. Model*. **1999**, 17, 57-61.
15. Balouiri, M.; Sadiki, M.; Ibnsouda, S.K. Methods for in vitro evaluating antimicrobial activity: A review. *J. Pharm. Anal*. **2016**, 6, 71-79.

16. Al burgus, A.F.; Ali, O.T.; Mohammad, O.Y. Synthesis and in vitro screening of benzo [*h*] coumarinyl heterocycles as promising antibacterial agents. *Bull. Chem. Soc. Ethiop*. **2024**, 38, 1815-1826.

17. Aliyu, H.N.; Suleiman, Z. Spectrophotometric analysis on anticonvulsant bis (N-isatin benzene-1-hydroxy-2-iminato) Mn(II), Fe(II) and Co(II) complexes. *Global Adv. Res. J. Microbiol.* **2012**, 1, 079-083.

18. Khan, Z.; Maqsood, Z.T.; Tanoli, M.A.K.; Khan, K.M.; Iqbal, L.; Lateef, M. Synthesis, characterization, in-vitro antimicrobial and antioxidant activities of Co^{+2}, Ni^{+2}, Cu^{+2} and Zn^{+2} complexes of 3-(2-(2-hydroxy-3-methoxybenzylidene) hydrazono) indolin-2-one. *Arab J. Basic Appl. Sci.* **2015**, 11, 125-130.

19. Mustafa, N.A.; Ahmed, S.A. Design, synthesis, characterization, DFT, molecular docking, and in vitro screening of metal chelates incorporating Schiff base. *Bull. Chem. Soc. Ethiop.* **2024**, 38, 1625-1638.

20. Kulkarni, P.A.; Habib, S.I.; Saraf, D.V.; Deshpande, M.M. Synthesis, spectral analysis and antimicrobial activity of some new transition metal complexes derived from 2,4-dihyroxy acetophenones. *Res. J. Pharm. Biol. Chem. Sci.* **2012**, 3, 107-113.

21. Wahba, O.; Hassan, A.M.; Naser, A.; Hanafi, A. Preparation and spectroscopic studies of some copper and nickel Schiff base complexes and their applications as colouring pigments in protective paints industry. *Egypt J. Chem*. **2017**, 60, 25-40.

22. Al-Assafe, A.Y.; Al-Quaba, R.A. Synthesis, characterization and antibacterial studies of ciprofloxaci-imines and their complexes with oxozirconium(IV), dioxomolybdenum(VI), and dioxotungsten(VI). *Bull. Chem. Soc. Ethiop*. **2024**, 38, 949-962.

23. Putaya, H.A.; Ndahi, N.P.; Bello, H.S.; Mala, G.; Osunlaja, A.A.; Garba, H. Synthesis, characterization and antimicrobial analysis of Schiff bases of *o*-phenylenediamine and 2-aminopyridine-3-carboxylic acid with ofloxacin and their metal(II) complexes. *Int. J. Biol. Chem. Sci.* **2020**, 14, 263-278.

24. Fedorowicz, J.; Sączewski, J. Modifications of quinolones and fluoroquinolones: Hybrid compounds and dual-action molecules. *Monatshefte für Chemie*. **2018**, 149, 1199-1245.

25. Al-burgus, A.F.; Ali, O.T.; Al-abbasy, O.Y. New spiro-heterocyclic coumarin derivatives as antibacterial agents: Design, synthesis and molecular docking. *CTA* **2024**, 11, 202411308.

26. Abu-Dief, A.M.; Alotaibi, N.H.; Al-Farraj, E.S.; Qasem, H.A.; Alzahrani, S.; Mahfouz, M.K.; Abdou, A. Fabrication, structural elucidation, theoretical, TD-DFT, vibrational calculation and molecular docking studies of some novel adenine imine chelates for biomedical applications. *J. Mol. Liq*. **2022**, 365, 119961.

27. Mohamed, G.G.; Mahmoud, W.H.; Refaat, A.M. Nano-azo ligand and its superhydrophobic complexes: Synthesis, characterization, DFT, contact angle, molecular docking, and antimicrobial studies. *J. Chem*. **2020**, 1, 6382037.